PCCP

Efficiency of ruthenium dye sensitized solar cell enhanced by 2,6-Bis[1-(phenylimino)ethyl]pyridine as co-sensitizer containing methyl substituents on its phenyl rings

Journal:	*Physical Chemistry Chemical Physics*
Manuscript ID:	CP-ART-09-2014-004240.R1
Article Type:	Paper
Date Submitted by the Author:	25-Oct-2014

Complete List of Authors:	Wei, Liguo; Harbin Institute of Technology, Na, Yong; Harbin Institute of Technology, Chemistry Yang, Yulin; Harbin Institute of Technology, Department of Chemistry Fan, Ruiqing; Harbin Institute of Technology , Wang, Ping; Harbin Institute of Technology, Li, Liang; Harbin Institute of Technology, Department of Applied Chemistry

Efficiency of ruthenium dye sensitized solar cell enhanced by 2,6-Bis[1-(phenylimino)ethyl]pyridine as co-sensitizer containing methyl substituents on its phenyl rings

Liguo Wei,[ab] Yong Na,*[a] Yulin Yang,*[a] Ruiqing Fan,[a] Ping Wang[a] and Liang Li[a]

[a]*Department of Chemistry, Harbin Institute of Technology, Harbin 150001, P.R. China.*

[b]*College of Environmental and Chemical Engineering, Heilongjiang University of Science and Technology, Harbin 150022, P.R. China.*

To whom the correspondence should be addressed.

Prof. Yulin Yang and Dr. Yong Na

Department of Chemistry

Harbin Institute of Technology, Harbin 150001, P. R. China

Fax: +86-451-86418270

E-mail: ylyang@hit.edu.cn and yongna@hit.edu.cn

2,6-bis[1-(phenylimino)ethyl]pyridine (M0) and its derivatives containing methyl groups on its phenyl rings (M1o, M1p and M2) are employed as co-sensitizers in dye-sensitized solar cells (DSSCs). The prepared co-sensitizers could alleviate the aggregation of ruthenium dye N719 on the TiO_2 film, enhance the spectral responses of the co-sensitized TiO_2 film in region from 400 to 750 nm, suppress the electron recombination, prolong the electron lifetime and decrease the total resistance of DSSCs. The number and position of the methyl groups are two key factors that play important roles in the performances of DSSCs. The optimized cell device co-sensitized by M1p/N719 dye gives a short circuit current density of 16.48 mA cm^{-2}, an open circuit voltage of 0.72 V and a fill factor of 0.62 corresponding to an overall conversion efficiency of 7.32% under standard global AM 1.5 solar irradiation, which is 35% higher than that of device solely sensitized by N719 under the same conditions.

Introduction

Dye-sensitized solar cells (DSSCs) have attracted much attention due to its low-cost and simple fabrication for conversion of the solar energy into electricity.[1] Since O'Regan and Grätzel first reported a ruthenium polypyridyl complex as the light harvesting unit in a DSSC device in 1991,[2] photoanodes based on ruthenium sensitizers have been extensively studied in order to develop high efficient solar cells. To address the problem that the light harvesting of ruthenium polypyridyl complexes are highly efficient at ca. 550 nm but falls away dramatically between 650 and 700 nm, extension of the absorption spectrum of a ruthenium dye by modification its ligands or fabrication of the co-sensitized photoanodes containing a ruthenium dye and another dye selected to absorb light from different parts of the solar spectrum has been reported.[3-7] In the condition that a single ruthenium dye is unable to fulfill all the requirements for obtaining an efficient device, co-sensitization is considered to be a more promising way. In the past decade, several kinds of dyes (ruthenium phthalocyanine dye, zinc porphyrin dye, organic dye etc.) were employed as co-sensitizers in combination of the ruthenium dyes,[8-19] and overall solar-to-electrical energy conversion efficiency of 11.0% has been achieved.[11]

The co-sensitization methods mentioned above were all focused on collocation of different dyes on the TiO_2 film for the complementary in their spectral responses. Besides the absorption breadth of dye sensitized film, its absorption intensity also plays a very important role in the performance of the cell.[4] However, the optical absorptivity of ruthenium dye-sensitized films improved by co-sensitization has attracted little attention. 2,6-bis[1-(phenylimino)ethyl]pyridine bonded to the TiO_2 surface potentially through its nitrogen atoms was found to function as this kind of co-sensitizer in our previous report.[20,21] Among the several co-sensitizers possessing alkyl groups on their phenyl rings, the one containing two dimethylphenyl groups was the most excellent.[14] In this context, we systematically introduce methyl groups to the phenyl rings of the 2,6-bis[1-(phenylimino)ethyl]pyridine, and the compounds noted as M0, M1o, M1p and M2 (Scheme 1) are employed as co-sensitizers in the well-known ruthenium N719 dye based solar cell. The effects of different numbers and positions of methyl groups in the structures of co-sensitizers on the photochemical performances of the cells have been investigated.

Results and discussions

Optical properties

The absorption spectra of M0, M1o, M1p and M2 in ethanol are shown in Fig. 1 and their absorption data are listed in Table 1. All of the four prepared compounds display strong absorption peaks at ca. 279 nm with weak shoulder absorption bands at around 335 nm. In comparison to the absorption of N719 in ethanol (shown in Fig. 1), the prepared compounds could only compensate for the absorption of N719 in the UV region from 320 nm to 360 nm, but not for that in the visible region. However, as shown in Fig. 2, the TiO_2 films co-sensitized by N719 and the prepared compounds led to surprising results on their absorption spectra in the visible region. The two clear absorption bands of N719 in ethanol solution at 383 and 525 nm are broadened into both sides when it attaches to TiO_2 film, indicating the formation of Herrings-bone aggregates by N719 on the TiO_2 nanocrystal surface. When anyone of the prepared four compounds is incorporated into the N719 sensitized TiO_2 film, the intensities of the two characteristic absorption bands both increase a lot. Besides, the two absorption bands at 554 and 367 nm attributed to N719 move to 547 and 375 nm, respectively, suggesting the aggregation degree of N719 on the TiO_2 film is decreased. The alleviation of aggregates adjusts the arrangement of N719 molecules toward a more uniform orientation and formed a compact layer with M0, M1o, M1p and M2, respectively. Apparently, the increment of the absorption intensity of the TiO_2 films after co-sensitization will contribute to their spectral responses as well as the power conversion efficiency of the DSSCs.

Electrochemical properties

The methyl-substituted phenyl rings in 2,6-bis[1-(phenylimino)ethyl]pyridine could be considered as donor parts and the pyridyl rings could be considered as acceptor parts. The two imino-conjugated groups can function as π-conjugated bridges, so the four prepared compounds are donor-π-conjugated-acceptor (D-π-A) type co-sensitizers. It is speculated that electrons may transfer from the prepared co-sensitizers to the TiO_2 conduction band. Therefore, cyclic voltammetry (CV) experiments were carried out to determine the highest occupied molecular orbital (HOMO) levels and the lowest unoccupied molecular orbital (LUMO) levels of the four prepared compounds and the experimental data are also summarized in Table 1. Based on their first oxidation potentials, the HOMO value for M0, M1o, M1p and M2 was calculated with following formula:[22]

$$E_{HOMO} = -(E^{ox}_{onset} + 4.4)(eV)$$

Where E_{onset}^{ox} is the first oxidation potentials of 2,6-bis[1-(phenylimino)ethyl]pyridine, and 4.4 eV is the value on the Fermi level for 0.0 V vs SCE.[23] Therefore, the HOMO value for M0, M1o, M1p and M2 are −5.19, −5.15, −5.06 and −5.07 eV, respectively. As calculated from the edge of absorption spectra, the excitation transition energy ($E_{0\text{-}0}$) for M0, M1o, M1p and M2 are 2.89, 2.95, 2.97 and 2.92 eV, respectively. Therefore, the LUMO levels of M0, M1o, M1p and M2, calculated from E_{HOMO} + $E_{0\text{-}0}$, are −2.30, −2.20, −2.09 and −2.15 eV, respectively. For efficient electron injection, the LUMO level of a sensitizer should lie above the energy level of the conduction band (CB) of the TiO_2 semiconductor (–4.40 eV vs vacuum) and its HOMO energy level should lie below the energy level of the I^-/I_3^- redox couple in the presence of 4-tert-butyl pyridine (–4.85 eV vs vacuum) for regeneration.[24] As shown in Fig. 3, the electron injection and sensitizer regeneration are thermodynamically feasible based on the energy levels of the prepared co-sensitizers.[25] Besides, their HOMO energy levels locate above that of N719, which could also contribute to the regeneration of N719 thermodynamically.

Photoelectrochemical performances of dye-sensitized solar cell

The four prepared compounds were employed as co-sensitizers to assemble co-sensitized DSSCs and the co-sensitized DSSCs were fabricated followed a stepwise co-sensitization procedure by sequentially immersing the TiO_2 electrode (with thickness of *ca.* 10 um) in separate solution of N719 and prepared compound. For comparison purpose, devices sensitized by the individual dyes of N719 were also fabricated under the same experimental conditions. The photocurrent-voltage (*J–V*) characteristic of the devices co-sensitized by M0/N719, M1o/N719, M1p/N719 and M2/N719 as well as solely sensitized by N719 under illumination (AM 1.5 G, 100mW cm^{-2}) are shown in Fig. 4, and the corresponding cells performance are summarized in Table 2. The individually N719 sensitized device was found to exhibit overall conversion efficiency (η) value of 5.43% (with J_{sc} = 12.61 mA/cm^2, V_{oc} = 0.71 V, and *FF* = 0.61), while the co-sensitized solar cell devices M0/N719, M1o/N719, M1p/N719 and M2/N719 showed η value of 5.76% (with J_{sc} = 13.09 mA/cm^2, V_{oc} = 0.71 V, and *FF* = 0.62), 6.16% (with J_{sc} = 14.41 mA/cm^2, V_{oc} = 0.69 V, and *FF* = 0.62), 7.32% (with J_{sc} = 16.48 mA/cm^2, V_{oc} = 0.72 V, and *FF* = 0.62), and 7.00% (with J_{sc} = 16.53 mA/cm^2, V_{oc} = 0.72 V, and *FF* = 0.59), respectively. The efficiencies of the devices co-sensitized by M0/N719, M1o/N719, M1p/N719 and M2/N719 are all higher than that of devices individually sensitized by N719. Especially, the cells co-sensitized by M1p and N719 exhibited the best overall conversion

efficiency (η) of 7.32%, which is 35% higher than that of cells individually sensitized by N719 (5.43%).

The higher η value of co-sensitized solar cell compared with the individually N719 sensitized devices, is attributed to the enhanced photovoltaic parameters J_{sc} and V_{oc}. Particularly, the enhanced J_{sc} value is ascribed to the enhanced IPCE response of the cell, since they are related by the equation:

$$J_{sc} = \int e\phi_{\text{ph.AM1.5G}}(\lambda)d\lambda$$

Where e is the elementary charge and $\phi_{\text{ph.AM1.5G}}$ is the photon flux at AM 1.5 G.[1,6] The IPCE spectra of different devices were collected in Fig. 5. It is found that co-sensitized with M0, M1o, M1p and M2, respectively, could enhance the spectral response of N719 on TiO_2 film in the whole visible region and consequently enhance the photocurrent performance. This means the co-sensitization of N719 and prepared compound has a significant synergy effect on light harvesting, electron injection and electron collection on TiO_2. Based on the IPCE and the absorption spectra, it could be conclude that the cell's higher J_{sc} in the case of co-sensitization is ascribed to the decreased aggregation degree of N719 on the TiO_2 film and its enhanced spectra response.

To investigate the anti-aggregation effect of M0, M1o, M1p and M2 mentioned above, a widely used anti-aggregation co-adsorbent, chenodeoxycholic acid (CDCA),[26-28] was also applied in N719 sensitized DSSCs with and without M0, M1o, M1p and M2, and the results are also list in Table 2. When CDCA was added to N719/TiO_2, an impressively high cell performance surpassing that of N719 (5.43%) was achieved: η, 6.03%; J_{sc}, 13.84 mA cm^{-2}; V_{oc}, 0.71 V; *FF*, 0.61 (Table 2). Obviously, as has been widely reported in the literature for various dye systems,[28-31] addition of CDCA hampers N719 aggregation and improves J_{sc}. Compared with this, when M0, M1o, M1p and M2 were employed as co-sensitizer to N719 sensitized solar cells, a similar results was obtained, which indicates that the anti-aggregation effect of M0, M1o, M1p and M2 was comparable with CDCA. While when CDCA was present in the co-sensitized devices of M0/N719, M1o/N719, M1p/N719 and M2/N719, device efficiency was not further improved. This may be attributed to the comparable anti-aggregation effect of CDCA with M0, M1o, M1p and M2, and more than proper amount of anti-aggregation co-adsorbent would not afford too much for performance enhancement.

Moreover, when the molecular structures of M0, M1o, M1p and M2 are considered, the introduction of methyl groups to the phenyl rings of 2,6-bis[1-(phenylimino)ethyl]pyridines

contributes a lot to the J_{sc} improvement. The more methyl substituents on the structures of co-sensitizers result in more increment of J_{sc}, which is in the order of M2/N719 > M1p/N719 > M1o/N719 > M0/N719 > N719. This may be resulted from their enhanced capability of electron injection into TiO_2 and anti-aggregation of N719. Of particular importance is that the J_{sc} of the device sensitized by M1p/M719 is much higher than that sensitized by M1o/N719 is presumably because M1p contains one methyl substituents on the para-positions of imine groups, which hardly disturb the coplanarity of π-conjugated system of 2,6-bis[1-(phenylimino)ethyl]pyridine but obviously change its the HOMO and LUMO levels, leading to stronger capability of electron injection into TiO_2 than that of M1o. The co-sensitizer M2 containing more methyl substituents and exhibits a higher J_{sc}, but the *FF* of the device sensitized by M2/N719 is less than that sensitized by M1p/N719, leading to a lower η value. In a word, the number and position of methyl in 2,6-bis[1-(phenylimino)ethyl]pyridine are two important factors in enhancing the performance of co-sensitized DSSCs.

Electrochemical impedance spectroscopy (EIS)

EIS analysis was used to study the interfacial charge transfer process in DSSCs co-sensitized by M0/N719, M1o/N719, M1p/N719, and M2/N719. The measurements were scanned from 0.1 to 100 kHz at room temperature with an applied bias voltage of −0.75 V. The Nyquist plots for the devices under dark condition are shown in Fig. 6a. The diameters of the medium-frequency semicircle increased when the co-sensitizers M0, M1p, and M2 were incorporation to the N719 sensitized solar cell device, implying that the recombination reaction between the conduction band electrons in TiO_2 film and electrolyte is better inhibited by co-sensitization.[32] The charge transfer resistances at the dye/TiO_2/electrolyte interface (recombination resistance, R_{rec}) lie in the order of M1p/N719 > M2/N719 > M0/N719 > N719> M1o/N719, which is consistent with the V_{oc} of the devices. Correspondingly, the devices sensitized by M1p/N719 and M2/N719 achieve the higher V_{oc} value. The Nyquist plots for the devices under standard AM1.5G solar irradiation are also shown in Fig. 6b. The large medium-frequency semicircles are assigned to the charge transfer processes at TiO_2/dye/electrolyte interface, whose radius are decreased after incorporation of the four co-sensitizers, suggesting a decrease of the electron transfer impedance at this interface. In order to further understand the complex charge transfer process in DSSCs, a physical model of the equivalent circuit, $R_s[C_1(R_1O)](R_2Q_2)$, has been proposed and shown in Fig. 7.[33] The symbols R and

C represent resistance and capacitance, respectively. R_1 and R_2 are the charge transfer resistance and R_s is series resistance. The symbol O that depends on the parameters $Y_{o,1}$ and B, accounts for a finite-length Warburg diffusion (Z_w). The symbol Q is the constant phase element (CPE, its parameters are $Y_{o,2}$ and n). The parameters obtained by fitting the impedance spectra of the devices measured under standard AM1.5 G solar irradiation to the equivalent circuit are listed in Table 3. The resistance R_1 and R_2 for the devices are estimated from the medium frequency large semicircle and the relatively high frequency small semicircle, respectively. Both the resistances R_1 (12.19 Ω) and R_2 (10.12 Ω) for the device co-sensitized by M1p/N719 are smaller than the others'. Consequently, its smallest series resistance R_s results in the highest η among the five devices.

Dark current measurement

Controlling the back electron transfer in DSSC is vital to enhance the solar energy-to-electricity conversion efficiency. Dark current measurement in DSSC cannot be related directly to the back electron transfer process, since the electrolyte concentration in the films and the potential distribution across the nanoporous electrode in dark are different than those under illumination.[34] However, a comparison of dark current between the investigated cells can provide useful information regarding the back electron transfer process. Therefore, dark current measurement of DSSCs has been considered as a qualitative technique to describe the extent of the back electron transfer.[35]

Fig. 8 shows the dark current–voltage characteristics of the DSSCs based on different photoelectrodes with the applied bias from 0 to +0.80 V. The onset of the dark current for individual N719 sensitized DSSC occurs at a bias about +0.40 V, with a subsequent dramatic increase of dark current with the increase of potential. In contrast, for the co-sensitized DSSCs, the onset potential shifted to about +0.50 V for M0/N719, M1p/N719 and M2/N719 and keep at about 0.40 V for M1o/N719; furthermore, the dark current of the co-sensitized DSSCs increased much slower than that of N719 sensitized DSSC when potential was greater than +0.50 V. In other words, under the same potential bias, when the potential was $\geqslant$0.4 V, the dark current for the co-sensitized DSSCs was noticeably smaller than that for the N719 sensitized DSSC. The increase of the onset potential and the reduction of the dark current demonstrated that M0, M1o, M1p and M2 successfully suppress the electron back reaction with I_3^- in the electrolyte by forming a compact layer with N719. This is critical to reduce the current leakage in DSSC and enhance its efficiency.

Meanwhile, the decreased of dark current caused an increase of V_{oc}, which supported the results of EIS under dark conditions.

Open-circuit voltage decay (OCVD)

The OCVD technique has been employed as a powerful tool to study interfacial recombination processes in the TiO_2 DSSCs between photoinjected electrons and the electrolyte in the dark.[36,37] It can provide some quantitative information on the electron recombination rate.

Fig. 9a shows the OCVD decay curves of the DSSCs based on different photoelectrodes. It was observed that the OCVD response of the DSSC with co-sensitized photoelectrode was much slower than that individually sensitized by N719, especially in the shorter time domain (within 15 s). Since the decay of the V_{oc} reflects the decrease in the electron concentration, which is mainly caused by the charge recombination,[38] the cell using the co-sensitized photoelectrode has a lower electron recombination rate than that of the cell individually sensitized by N719.

Electron lifetime (τ_n) was proposed to quantify the extent of electron recombination with the redox electrolyte and has been proven effective. τ_n was calculated with the OCVD results in Fig. 9a according to the following equation:[39]

$$\tau_n = -\frac{K_B T}{e}\left(\frac{dV_{oc}}{dt}\right)^{-1}$$

where K_B is the Boltzmann constant, T is absolute temperature, e is the electronic charge, and dV_{oc}/dt is the derivative of the transient open-circuit voltage. Fig. 9b compares the results of the dependence of τ_n on the open-circuit voltage for DSSCs with and without the co-sensitized photoelectrode. It clearly demonstrates that, at any given open-circuit potential, the electron lifetime of the co-sensitized cell was longer than that of the cell individually sensitized by N719. The difference in OCVD was mainly due to the blocking effect of the compact layer made by co-sensitizers and N719. This suggests that the electrons injected from excited dye can survive longer and hence can facilitate electron transport without undergoing losses at the bare FTO surface. In conclusion, the OCVD measurements in Fig. 9 demonstrated that co-sensitizing with 2,6-bis[1-(phenylimino)ethyl]pyridine and its derivatives was able to reduce the photoelectron recombination speed effectively and prolong the lifetime of the photoelectrons.

Conclusions

We have developed and systematically investigated 2,6-bis[1-(phenylimino)ethyl]pyridine (M0) and

its derivatives (M1o, M1p and M2) as co-sensitizers in ruthenium dye N719 based solar cell. The co-sensitization could enhance the spectral response of the N719 dye sensitized TiO_2 film, suppress the electron recombination, prolong the electron lifetime and decrease the total resistance of DSSCs. Introduction of methyl groups to the phenyl rings of 2,6-bis[1-(phenylimino)ethyl]pyridine raises its HOMO levels and LUMO levels, which improves their capability of electron injection into TiO_2 and regeneration of N719, and consequently enhance the performances of the solar cell devices. The more methyl groups in the co-sensitizers make more improvements in J_{sc} value, but the position of the methyl group play decisive role in the power conversion efficiency since the co-sensitizer containing methyl groups on the para-position of imine groups not only improve the J_{sc} but also resulted in high *FF*. Finally, the device co-sensitized by M1p/N719 yields the overall efficiency of 7.32%, which is 35% higher than that of the device only sensitized by N719 (5.43%). This way of simple co-sensitization is a potential method that deserves to be further developed for high efficient DSSC fabrication.

Experimental section

Materials

2,6-Bis[1-(phenylimino)ethyl]pyridines (M0, M1o, M1p and M2) were prepared according to our previous report.[40,41] Cis-bis(isothiocyanato)bis(2,2-bipyridyl-4,4-dicarboxylato)-ruthenium(II)bis-tetrabutylammonium (N719) was obtained from Solaronix. All of the other chemicals and solvents in this work were used as received without further purification.

Spectroscopic measurements

UV-visible absorption spectra were recorded on SPECORD S600 spectrophotometer (Jena, Germany) for samples in ethanol solution and UV-2250 spectrophotometer (Shimadzu, Japan) for sensitized TiO_2 films, respectively.

Electrochemical measurements

Cyclic voltammograms were recorded using a CHI660D electrochemical potentiostat. The measurements were carried out in a three-electrode cell under argon. The working electrode was a planar platinum working electrode and the auxiliary electrode was a platinum wire. The reference electrode was a saturated calomel reference electrode in saturated KCl solution. A solution of 0.1 M

$TBAPF_6$ in dry ethanol was used as electrolyte. The electrolyte solution was degassed by bubbling with dry argon for 10 min before measurement.

Devices fabrication

TiO_2 paste for screen printing was prepared according to the literature.[42] It was printed onto conductive glass (FTO, 15 Ω $sq.^{-1}$, 90% transmittance in the visible, NSG, Japan) and then dried at 100 ºC for 5 min. The above process was repeated for six times. The obtained TiO_2 film was then sintered at 500 ºC for 15 min. Stepwise co-sensitization of the TiO_2 film was accomplished by dipping it in various solutions for different time intervals at room temperature. Typically, the photoanode was immersed in a solution of 0.3 mM M0 in absolute ethanol for 2 h and then washed with ethanol. It was further immersed in a solution of 0.3 mM N719 in absolute ethanol for 12 h and then washed with ethanol. For the co-adsorbed solar cells, chenodeoxycholic acid (CDCA) was added into the dye solutions at a concentration of 10mM. The sandwich-type solar cell device was assembled by placing a platinum-coated conductive glass as counter electrode on the co-sensitized photoanode, a drop of liquid electrolyte containing 0.5 M LiI, 0.05 M I2, 0.1 M 4-tert-butylpyridine (TBP) was added to fill the void between two electrodes and clipped together as open cells for measurement.

Photoelectrochemical measurements

Photocurrent-photovoltage (*I-V*) curves were recorded by Keithley model 2400 digital source meter under AM1.5 irradiation. The incident light intensity was 100 mW cm^{-2} calibrated by a standard silicon solar cell. The working areas of the cells were masked to 0.16 cm^{-2}. The measurement of the incident photon-to-current conversion efficiency (IPCE) was performed by an EQE/IPCE spectral response system (Newport).

Devices Characterizations

Electrical impedance spectroscopy (EIS), dark current and open-circuit voltage decay (OCVD) were recorded by CHI660D Electrochemical Analyzer. The measurements of EIS were taken over a frequency range of 0.1-100 kHz under standard global AM1.5 solar irradiation (100 mW cm^{-2}) or in the dark by applying a forward bias of –0.75V. The OCVD experiment is conduct by monitoring the subsequent decay of V_{oc} after stopping the illumination on DSSCs under open-circuit conditions.

Acknowledgements

This work was supported by National Natural Science Foundation of China (Grant 21171044 and 21371040), the National key Basic Research Program of China (973 Program, No. 2013CB632900), the Fundamental Research Funds for the Central Universities (Grant No. HIT. IBRSEM. A. 201409), and Program for Innovation Research of Science in Harbin Institute of Technology (PIRS of HIT No. A201418, A201416 and B201414).

Notes and references

1 A. Hagfeldt, G. Boschloo, L. Sun, L. Kloo and H. Pettersson, *Chem. Rev.*, 2010, **110**, 6595–6663.

2 B. O'Regan and M. Grätzel, *Nature*, 1991, **353**, 737–740.

3 J. H. Yum, E. Baranoff, S. Wenger, M. K. Nazeeruddin and M. Grätzel, *Energy Environ. Sci.*, 2011, **4**, 842–857.

4 F. Gao, Y. Wang, D. Shi, J. Zhang, M. K. Wang, X. Y. Jing, R. Humphry-Baker, P. Wang, S. M. Zakeeruddin and M. Grätzel, *J. Am. Chem. Soc.*, 2008, **130**, 10720–10728.

5 M. K. Nazeeruddin, F. D. Angelis, S. Fantacci, A. Selloni, G. Viscardi, P. Liska, S. Ito, B. Takeru and M. Grätzel, *J. Am. Chem. Soc.*, 2005, **127**, 16835–16847.

6 G. D. Sharma, G. E. Zervaki, P. A. Angaridis, A. Vatikioti, K. S. V. Gupta, T. Gayathri, P. Nagarjuna, S. P. Singh, M. Chandrasekharam, A. Banthiya, K. Bhanuprakash, A. Prtrou and A. G. Coutsolelos, *Organic Electronics*, 2014, **15**, 1324–1337.

7 G. D. Sharma, S. P. Singh, P. Nagarjuna, J. A. Mikroyannidis, R. J. Ball and R. Kurchania, *J. Renewable Sustainable Energy*, 2013, **5**, 043107.

8 J. N. Clifford, E. Palomares, M. K. Nazeeruddin, R. Thampi, M. Grätzel and J. R. Durrant, *J. Am. Chem. Soc.*, 2004, **126**, 5670–5671.

9 M. Mojiri-Foroushani, H. Dehghani and N. Salehi-Vanani, *Electrochimica Acta*., 2013, **92**, 315–322.

10 P. J. Holliman, M. Mohsen, A. Connell, M. L. Davies, K. Al-Salihi, M. B. Pitak, G. J. Tizzard, S. J. Coles, R. W. Harringston, W. Clegg, C. Serpa, O. H. Fontes, C. Charbonneau and M. J. Carnie, *J. Mater. Chem.*, 2012, **22**, 13318–13327.

11 L. Y. Han, A. Islam, H. Chen, C. Malapaka, B. Chiranjeevi, S. F. Zhang, X. D. Yang and M. Yanagida, *Energy Environ. Sci.*, 2012, **5**, 6057–6060.

12 H. Ozawa, R. Shimizu and H. Arakawa, *RSC Adv.*, 2012, **2**, 3198–3200.

13 K. M. Lee, Y. C. Hsu, M. Ikegami, T. Miyasaka, K. R. J. Thomas, J. T. Lin and K. C. Ho, *J. Power Sources,* 2011, **196**, 2416–2421.

14 S. Fan, C. Kim, B. Fang, K. Liao, G. Yang, C. Li, J. J. Kim and J. Ko, *J. Phys. Chem. C*, 2011, **115**, 7747–7754.

15 P. J. Holliman, M. L. Davies, A. Connell, B. Vaca Velasco and T. M. Watson, *Chem. Commun.*, 2010, **46**, 7256–7258.

16 G. D. Sharma, D. Daphnomili, K. S. V. Gupta, T. Gayathri, S. P. Singh, P. A. Angaridis, T. N. Kitsopoulos, D. Tasis and A. G. Coutsolelos, *RSC Adv.*, 2013, **3**, 22412–22420.

17 G. D. Sharma, S. P. Singh, R. Kurchania and R. J. Ball, *RSC Adv.*, 2013, **3**, 6036–6043.

18 S. P. Singh, M. Chandrasekharam, K. S. V. Gupta, A. Islam, L. Han and G. D. Sharma, *Organic Electronics*, 2013, **14**, 1237–1241.

19 G. D. Sharma, M. S. Roy and S. P. Singh, *J. Mater. Chem.*, 2012, **22**, 18788–18792

20 Y. Harima, T. Fujita, Y. Kano, I. Imae, K. Komaguchi, Y. Ooyama and J. Ohshita, *J. Phys. Chem. C,* 2013, **117**, 16364–16370.

21 L. Wei, Y. Yang, R. Fan, P. Wang, L. Li, J. Yu, B. Yang and W. Cao, *RSC Adv.*, 2013, **3**, 25908–25916.

22 C. M. Cardona, W. Li, A. E. Kaifer, D. Stockdale and G. C. Bazan, *Adv. Mater.*, 2011, **23**, 2367–2371.

23 D. M. de Leeuw, M. M. J. Simenon, A. R. Brown and R. E. F. Einerhand, *Synth. Met.*, 1997, **87**, 53–59.

24 G. Boschloo, L. Ha1ggman and A. Hagfeldt, *J. Phys. Chem. B,* 2006, **110**, 13144–13150.

25 K. R. J. Thomas, Y. C. Hsu, J. T. Lin, K. M. Lee, K. C. Ho, C. H. Lai, Y. M. Cheng and P. T. Chou, *Chem. Mater.*, 2008, **20**, 1830–1840.

26 X. Jiang, T. Marinado, E. Gabrielsson, D. P. Hagberg, L. Sun and A. Hagfeldt, *J. Phys. Chem. C*, 2010, **114**, 2799–2805.

27 P. Salvatori, G. Marotta, A. Cinti, C. Anselmi, E. Mosconi and F. De Angelis, *J. Phys. Chem. C*, 2013, **117**, 3874–3887.

28 J. H. Yum, S. J. Moon, R. H. Baker, P. Walter, T. Geiger, F. Nüesch, M. Grätzel and M. K. Nazeeruddin, *Nanotechnology*, 2008, **19**, 424005.

29 G. Cicero, G. Musso, A. Lambertini, B. Camino, S. Bianco, D. Pugilese, F. Risplendi, A. Sacco,

N. Shahzad, A. M. Ferrari, B. Ballarin, C. Barolo, E. Tresso and G. Caputo, *Phys. Chem. Chem. Phys.*, 2013, **15**, 7198–7203.

30 T. Maeda, S. Mineta, H. Fujiwara, H. Nakao, S. Yagi and H. Nakazumi, *J. Mater. Chem. A*, 2013, **1**, 1303–1309.

31 M. G. Iglesias, J. J. Cid, J. H. Yum, A. Forneli, P. Vazquez, M. K. Nazeeruddin, E. Palomares, M. Grätzel and T. Torres, *Energy Environ. Sci.*, 2011, **4**, 189–194.

32 W. Zhang, R. Zhu, X. Liu, B. Liu and S. Ramakrishna, *Appl. Phys. Lett.*, 2009, **95**, 043304.

33 K. Mukherjee, T. Teng, R. Jose and S. Ramakrishna, *Appl. Phys. Lett.*, 2009, **95**, 012101.

34 A. Zaban, A. Meier and B. A. Gregg, *J. Phys. Chem. B*, 1997, **101**, 7985–7990.

35 S. Ito, P. Liska, P. Comte, R. Charvet, P. Pechy, U. Bach, L. Schmidt-Mende, S. M. Zakeeruddin, A. Kay, M. K. Nazeeruddin and M. Graetzel, *Chem. Commun.*, 2005, **25**, 4351–4353.

36 J. Bisquert, A. Zaban, M. Greenshtein and I. Mora-Sero, *J. Am. Chem. Soc*., 2004, 1**26**, 13550–13559.

37 K. Fan, W. Zhang, T. Y. Peng, J. N. Chen and F. Yang, *J. Phys. Chem. C*, 2011, **115**, 17213–17219.

38 H. Yua, S. Q. Zhang, H. J. Zhao, G. Willb and P. Liu, *Electrochim. Acta*, 2009, **54**, 1319–1324.

39 A. Zaban, M. Greenshtein and J. Bisquert, *ChemPhysChem*, 2003, **4**, 859–864.

40 R. Fan, D. Zhu, Y. Mu, G. Li, Y. Yang, Q. Su and S. Feng, *Eur. J. Inorg. Chem.*, 2004, 4891–4807.

41 R. Fan, H. Chen, P. Wang, Y. Yang, Y. Yin and W. Hasi, *J. Coord. Chem.*, 2010, **63**, 1514–1530.

42 P. Y. Reddy, L. Giribabu, C. Lyness, H. J. Snaith, C. Vijaykumar, M. Chandrasekharam, M. Lakshmikantam, J. H. Yum, K. Kalyanasundaram, M. Grätzel and M. K. Nazeeruddin. *Angew. Chem. Int. Ed.*, 2007, **46**, 373–376.

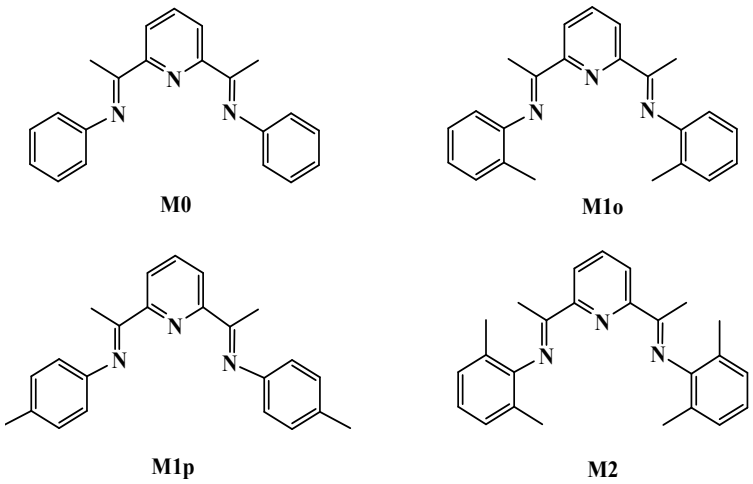

Scheme 1 Molecular structures of M0, M1o, M1p and M2.

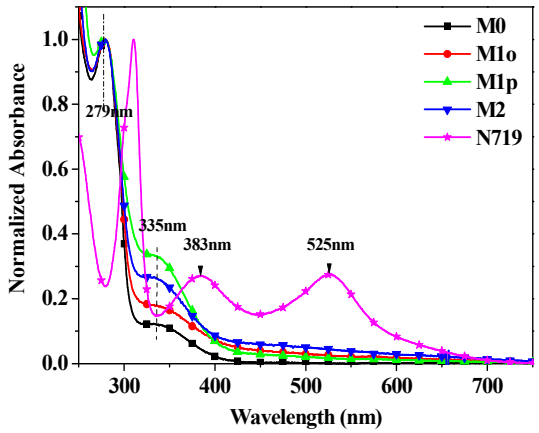

Fig. 1 UV-visible absorption spectra of 2,6-bis[1-(phenylimino)ethyl]pyridines and N719 in ethanol.

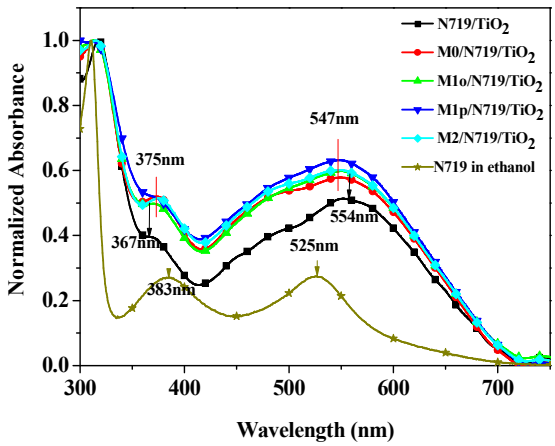

Fig. 2 UV-visible absorption spectra of different photoelectrodes.

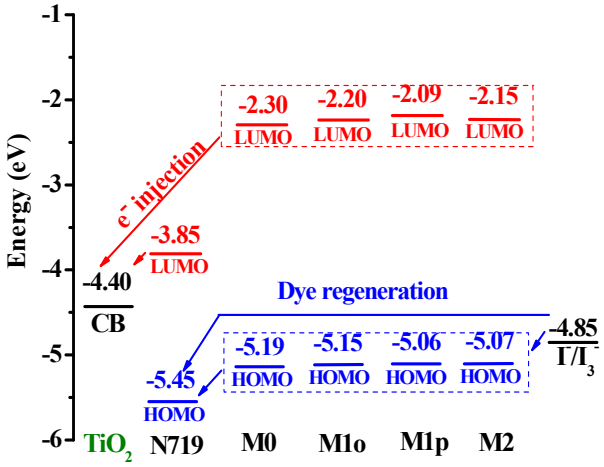

Fig. 3 Energy levels of co-sensitizers and of the other materials used for DSSCs fabrication.

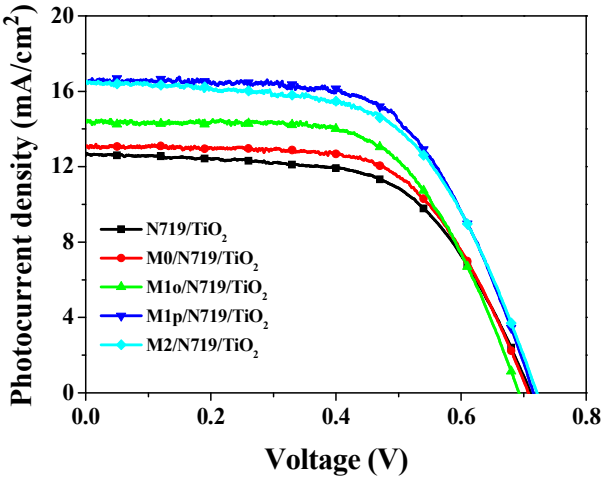

Fig. 4 *J-V* curves for DSSCs based on co-sensitized photoelectrodes and N719 sensitized photoelectrode.

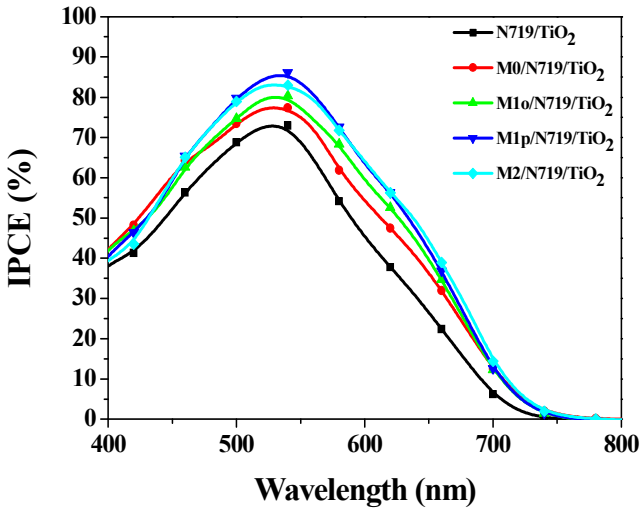

Fig. 5 IPCE spectra of DSSCs based on single N719 sensitized and co-sensitized photoelectrodes.

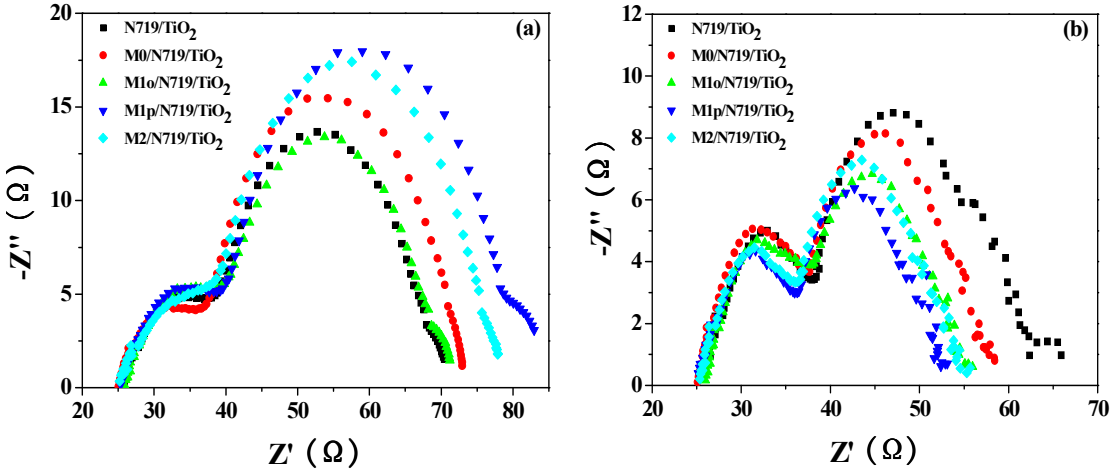

Fig. 6 Nyquist plots of DSSCs based on different photoelectrodes measured (a) in dark, (b) under standard AM1.5G solar irradiation.

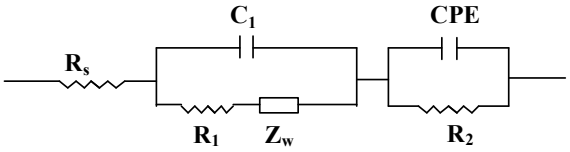

Fig. 7 Equivalent circuit used to represent interface in DSSCs consisting of FTO glass substrate/TiO_2/Dye/I_3^-/I^-‖Pt/FTO glass substrate.

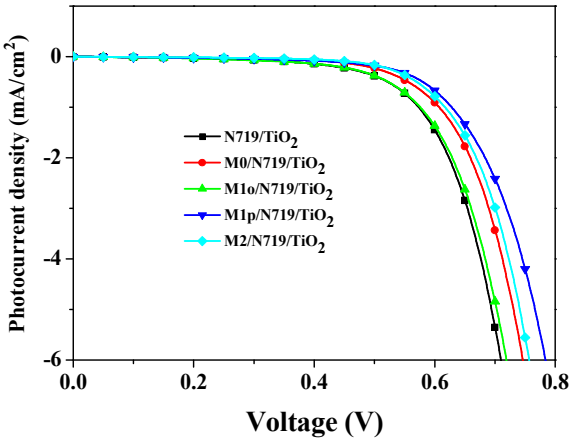

Fig. 8 Dark current of the DSSCs based on different photoelectrodes.

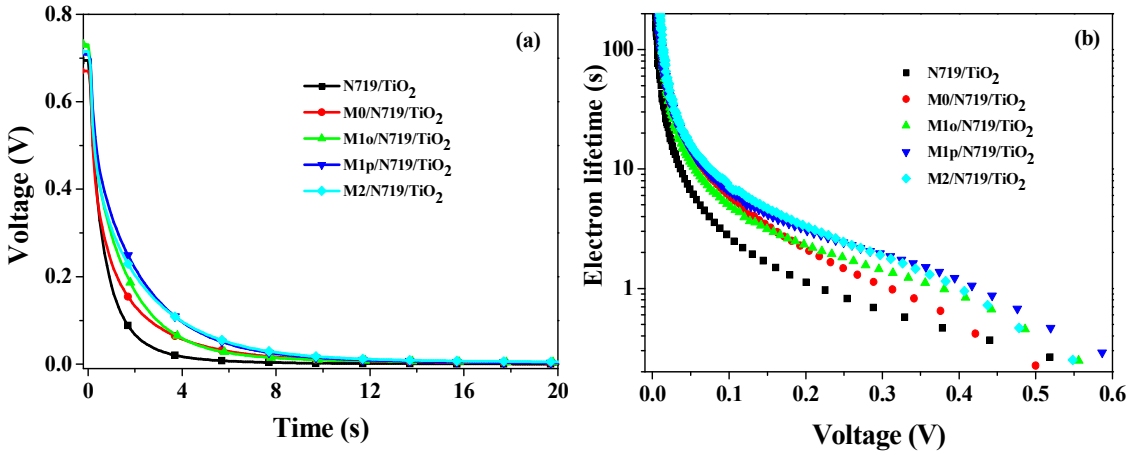

Fig. 9 (a) Open-circuit voltage decay curves of the DSSCs based on different photoelectrodes. (b) Comparison of electron lifetime as a function of open-circuit voltage of DSSCs based on different photoelectrodes.

Table 1

Experimental data for spectral and electrochemical properties of co-sensitizers.

Co-sensitizers	λ_{abs}(nm)[a]	$\varepsilon(M^{-1}cm^{-1})$[a]	E_{ox}(V vs SCE)[b]	$E_{0\text{-}0}$(eV)[c]	E_{HOMO}(eV)[d]	E_{LUMO}(eV)[d]
M0	277	26025	0.79	2.89	-5.19	-2.30
M1o	278	26335	0.75	2.95	-5.15	-2.20
M1p	279	26522	0.66	2.97	-5.06	-2.09
M2	280	26428	0.67	2.92	-5.07	-2.15

[a] Absorption spectra were recorded in ethanol solution (3×10^{-4} M) at room temperature.

[b] The first oxidation potentials of compounds were obtained by CV measurement.

[c] Optical band gap calculated from the absorption spectra edge.

[d] The values of E_{HOMO} and E_{LUMO} were calculated with the following formula:

$E_{HOMO} = -(E^{ox}_{onset} + 4.4)(eV)$; $E_{LUMO} = E_{HOMO} + E_{0\text{-}0}$ [22]

where $E_{0\text{-}0}$ is the absorption edge of co-sensitizers.

Table 2 Performances of DSSCs based on different photoelectrodes.

Photoelectrode	J_{sc} **(mA/cm^2)**	V_{oc} **(V)**	***FF***	η **(%)**
N719/TiO$_2$	12.61	0.71	0.61	5.43
M0/N719/TiO$_2$	13.09	0.71	0.62	5.76
M1o/N719/TiO$_2$	14.41	0.69	0.62	6.16
M1p/N719/TiO$_2$	16.48	0.72	0.62	7.32
M2/N719/TiO$_2$	16.53	0.72	0.59	7.00
CDCA+N719/TiO$_2$	13.84	0.71	0.61	6.03
CDCA+M0/N719/TiO$_2$	14.28	0.69	0.60	5.91
CDCA+M1o/N719/TiO$_2$	14.11	0.70	0.62	6.38
CDCA+M1p/N719/TiO$_2$	16.58	0.73	0.59	7.23
CDCA+M2/N719/TiO$_2$	16.56	0.70	0.60	6.93

Table 3 Parameters obtained by fitting the impedance spectra of solar cells measured under standard AM1.5 G solar irradiation using the equivalent circuit.

				O			Q_2	
DSSC samples	R_s (Ω)	C_1 (10^{-4} F)	R_1 (Ω)	$Y_{O,1}$ (10^{-1} S)	B ($S^{1/2}$)	R_2 (Ω)	$Y_{O,2}$ ($10^{-5}S^{1/2}$)	n
N719/TiO$_2$	25.60	6.24	15.56	1.38	0.50	14.10	9.03	0.76
M0/N719/TiO$_2$	25.69	5.75	16.44	0.877	0.68	13.04	10.10	0.73
M1o/N719/TiO$_2$	25.20	7.03	14.19	1.47	0.59	13.06	7.39	0.77
M1p/N719/TiO$_2$	24.67	7.57	12.19	1.35	0.65	10.12	10.40	0.72
M2/N719/TiO$_2$	25.58	7.39	12.33	1.34	0.51	11.43	8.99	0.75